Optimization of optical limiting devices based on excited-state absorption

Tiejun Xia, David J. Hagan, Arthur Dogariu, Ali A. Said, and Eric W. Van Stryland

Limiting devices protect sensitive optical elements from laser-induced damage (LID). Passive devices use focusing optics to concentrate the light through a nonlinear optical (NLO) element (or elements) to reduce the limiting threshold. Unfortunately, these NLO elements may themselves undergo LID for high inputs, restricting the useful dynamic range (DR). Recently, efforts at optimizing this DR have focused on distributing the NLO material along the propagation path z of a focused beam, resulting in different portions of the device (in z) exhibiting NLO response at different inputs. For example, nonlinear absorbers closer to the lens, i.e., upstream, protect device elements downstream near the focal plane. This results in an undesirable increase in the threshold, although the lowest threshold is always obtained with the final element at focus. Thus there is a compromise between DR and threshold. This compromise is determined by the material. We concentrate on reverse saturable absorber (RSA) materials (molecules exhibiting larger excited-state than ground-state absorption). We look at both tandem devices and devices in which the concentration of the NLO material is allowed to spatially vary in z. These latter devices require solid-state hosts. The damage threshold of currently available solid-state hosts is too low to allow known RSA materials to reach their maximum absorption, which occurs when all molecules are in their excited state. This is demonstrated by approximate analytical methods as well as by a full numerical solution of the nonlinear wave propagation equation over extremely large distances in z (up to $10^3 \, Z_0$, where Z_0 is the Rayleigh range of the focused beam). The numerical calculations, based on a one-dimensional fast Fourier transform, indicate that proper inclusion of diffraction reduces the effectiveness of reverse saturable absorption for limiting, sometimes by more than a factor of 10. Liquid-based devices have higher damage thresholds (damage occurs to the cuvette wall) and, thus, larger nonlinear absorption. However, RSA material in liquid hosts may suffer from larger thermal lensing. © 1997 Optical Society of America

1. Introduction

Considerable effort has been expended to devise passive means of protecting sensitive detection systems from damage caused by high-power laser beams.[1,2] Here passive implies that the optical energy is used directly in a nonlinear material to cause the material to absorb, refract, deflect, or scatter the beam at high-input energies or powers. To date no materials have exhibited strong enough nonlinear response to show limiting without optical gain, i.e., focusing to concentrate the light in the material. Although the strongest nonlinear response will be obtained by placing the nonlinear material at focus, from a practical viewpoint, the material is also most likely to undergo laser-induced damage at this position, which can result in a small dynamic range (DR). The DR is defined as the linear transmittance divided by the lowest transmittance, which occurs at high inputs. For liquid-based limiters this may actually help limiting, in that the resulting plasma may block incoming light.[3] However, solid-state hosts undergo irreversible damage as do the optical cells that hold liquid limiter materials.[4] This has prompted researchers to devise means of protecting the limiter itself from damage by placing nonlinear material in front of focus, thus increasing the DR. Various methods have been used, including the semiconductor self-protecting monolithic optical power limiter or MONOPOL[5,6] and tandem optical limiters[7–11] that use discrete nonlinear elements of one or more types. Here we explore two similar geometries, tandem[10]
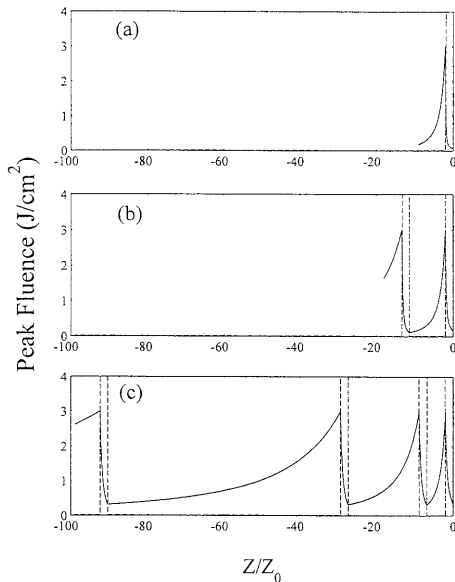
Fig. 1. On-axis fluence as a function of propagation distance for (a) a single-element limiter, (b) a two-element tandem limiter, and (c) a four-element limiter at maximum input energy. Each limiter uses the same nonlinear material, with concentrations adjusted so that the overall limiter transmittance is the same in each case.

and graded density,[11] for devices. We concentrate on the use of excited-state absorber (ESA) materials for these devices, although the geometries are applicable to other nonlinear materials.

Molecules exhibiting excited-state absorption have received considerable attention as promising candidates for use in passive optical limiters.[7,12,13] For such materials the ESA cross section is larger than that of the ground state, causing the absorption to increase with input fluence F (energy per unit area). For this reason, they are often referred to as reverse saturable absorber (RSA) materials.[14] In an effort to increase the DR of limiting devices, Hagan et al.[8] presented a combined experimental and theoretical study of discrete-element tandem ESA limiters. In this analysis, it was assumed that one element was placed at focus, while others were placed upstream in such a way that the maximum output energy E_{max} of one element was equal to the maximum input energy (the damage energy) E_d of the next. This criterion yields the positions of each element, and it was shown that the DR for such a limiter is given, in this simplified model, by the product of the DR's of the individual elements. The principle is illustrated in Fig. 1, where the on-axis fluence distribution is plotted as a function of the propagation distance z for (a) single-element, (b) two-element, and (c) four-element tandem limiters, each with an overall linear transmittance of 54%. Here, for clarity, it is assumed that all elements have identical nonlinearity, but with the concentration adjusted so that each composite limiter has the same overall transmittance, and all elements have the same damage threshold fluence F_d. In Fig. 1, $F_d = 3$ J/cm². Also for simplicity, this calculation assumes that the beam shape

is undistorted by the nonlinear absorption or any other effect. Figure 1 illustrates how the tandem limiter uses the focusing of the beam to keep the fluence high enough to generate significant excited-state absorption while the nonlinear loss balances the focusing to keep the fluence below the damage threshold. We clearly can see that the greater the number of elements, the higher the average fluence through the length of each element. This results in more optimized limiting as discussed below.

Recently, Miles[11] showed how the tandem limiter principle can theoretically be carried to the limit where the on-axis fluence is kept constant just below the damage fluence F_d over the entire length of the limiter in z by using a nonuniform concentration (or graded density) of ESA material. Because it allows the maximum fluence level at all points through the limiter, this design produces the largest excited-state absorption for any given F_d. This also results in the largest possible DR. In the same paper, a more generalized tandem limiter design was presented in which the final element need not be at focus. For a fixed linear transmittance, however, the lowest transmitted energy always occurs with the final element at focus.

In this paper, we present a detailed analysis of the behavior of ESA materials described by a five-level molecular model. We use the results to give both approximate analytical solutions for tandem devices and graded density devices [following Miles (Ref. 11)] as well as full numerical solutions of the nonlinear propagation of the electric field for such devices. The approximate analytical model carefully includes the role of the excited-state population and shows that considerably higher fluences than previously reported[11] are needed to fully populate this level. Thus the operating fluences needed to optimize devices are higher than previously expected. Results using the beam-propagation code, which is capable of calculating nonlinear propagation over long distances for focused beams, show that proper inclusion of diffraction results in a further reduction in limiting as compared with analytical models that are based on the assumption of constant-shape beam propagation. This reduced limiting gives as much as an order-of-magnitude reduction in the expected DR. These results indicate the importance of full numerical modeling in the design of optical limiting devices.

If the excited state of a RSA material could be fully populated to obtain the maximum possible absorption, i.e., full saturation of the ground-state absorption, the design and analysis of optimized limiters would be relatively simple. However, this is not seen to be the case. Currently known ESA materials are only partially saturated near the damage threshold of the host. In most materials the complexity is compounded by the presence of more than one ESA process. It has been shown experimentally that at high fluence levels for nanosecond pulses, a five-level model[12] is needed to describe the material response. Because the performance criteria (e.g., DR) are set at fluences close to the damage threshold,

the estimation of performance and limiter design depend on a correct analysis of the nonlinear response of ESA materials at high fluence. Here we provide this analysis in the approximation that nonlinear refraction may be neglected. A discussion of the possible effects of nonlinear refraction is included in the conclusions. The analytical design of the graded density limiter of Ref. 11 requires a three-level ESA model, although this is not an accurate physical description of most ESA materials at high fluence. Therefore, in Section 2, we present a quasi three-level model for organic dyes exhibiting excited-state absorption and discuss the limitations of such a model. In Section 3 we describe how temporal averaging over the optical pulse gives an effective ESA cross section for the graded density limiter, whereas for the tandem limiter, spatial integration in z through the limiting element must also be performed to find another effective absorption cross section. Both spatial (in z and radial in r) and temporal (in t) irradiance variations make it difficult to fully populate the excited state (at all z, t, and r) while keeping the pulse below the damage threshold at all points in the limiter. This prompts the designer to use a material with as high a damage threshold as possible. In Section 4, we describe the constraints that a constant fluence design imposes on limiter performance. We then compare graded and tandem limiter systems with particular attention to the damage threshold of these materials, including hosts and containment vessels. This is followed by the analytical design of a high DR limiter. This design of an optimized limiter is based on the assumption that the beam shape remains undistorted on propagating through the nonlinearly absorbing material, an apparently gross assumption given that the beam size may change by several orders of magnitude. It is therefore necessary to check the analytic predictions with a numerical beam-propagation code. Section 5 describes this beam-propagation model and its application to graded density limiters. We also describe how we can use the nonlinear propagation code to determine a numerically modified molecular density distribution that keeps the on-axis fluence constant, while properly including the effects of diffraction. We also examine a numerical analysis of the tandem limiter design. In the conclusion, we discuss other factors, particularly thermal lensing, which will need to be accounted for to refine further the design of practical limiting devices.

2. Excited-State Absorber Models

In the excited-state absorption process, weak absorption from the ground state results in population of excited states having a larger absorption cross section and hence an overall decrease in transmittance. Limiting properties of many such materials, for example, metallo-phthalocyanines,[7,12–14] have been studied in detail, resulting in a five-band model for the nonlinear absorption process, depicted schematically in Fig. 2. The system is more correctly described by a band model rather than a level model.
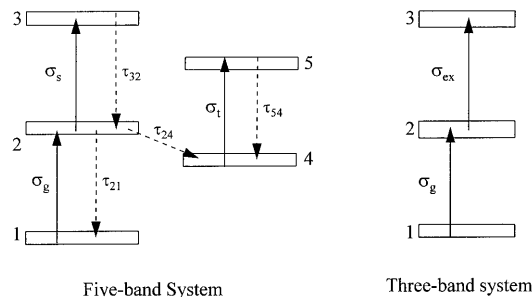

Fig. 2. Five-level model of excited-state absorption and equivalent quasi three-level model.

For example, linear absorption involving transitions from the ground state to the S_1 band usually result in excitation high into the S_1 vibration–rotation manifold. This is followed by rapid decay to the bottom of the band, whereupon the molecule is placed in an energy state far from resonance with the incident radiation. This allows complete depletion of the ground state and population of S_1. As the decay between singlet and triplet states is spin forbidden, decay from the lowest triplet-state (T_1) decay to the ground state (S_0) (well removed in energy) is negligible on the time scale of typical high-power Q-switched laser pulse widths (≈ 10 ns) that limiters are designed to protect against. However, spin–orbit coupling induced by the metal substitute in metallo-phthalocyanines or metallo-naphthalocyanines, along with the closeness in energy of the S_1 and T_1 levels, causes the lifetime of the S_1 to T_1 transition to be of the order of nanoseconds. For all but very high irradiance calculations, we find that we can neglect the populations of bands three and five. Including all of the above considerations, the system can then be described by the following rate equations (see Fig. 2):

$$\frac{\partial N_1}{\partial t} = -\frac{\sigma_g I}{\hbar \omega} N_1 + \frac{N_2}{\tau_{21}}, \tag{1a}$$

$$\frac{\partial N_2}{\partial t} = \frac{\sigma_g I}{\hbar \omega} N_1 - \frac{N_2}{\tau_2}, \tag{1b}$$

$$\frac{\partial N_4}{\partial t} = \frac{N_2}{\tau_{24}}, \tag{1c}$$

$$N_0 = N_1 + N_2 + N_4, \tag{1d}$$

$$\frac{\partial I}{\partial z} = -(\sigma_g N_1 + \sigma_s N_2 + \sigma_t N_4)I, \tag{1e}$$

where N_j is the population per cubic centimeter of band j and the overall lifetime τ_2 of band two is given by $\tau_2^{-1} = \tau_{21}^{-1} + \tau_{24}^{-1}$. In some of the materials studied,[9] the triplet–triplet transition cross section σ_t is larger than the excited singlet-state transition cross section σ_s. Consequently the nonlinear behavior changes with input fluence and pulse width. However, if a single pulse width is to be considered, we can use a quasi three-level system as shown in Fig. 2. This has a ground-state absorption cross sec-

tion σ_g and a single ESA cross section σ_{ex}, and is found to agree well with the full five-band model (for a single pulse width) and hence can often give good agreement with limiting and Z-scan[15] data taken on single-element thin samples of RSA material. Replacing σ_{ex} with σ_t[11] usually results in an overestimation of the limiter performance as σ_t is often greater than σ_s. To correctly determine this effective σ_{ex} for a given material, fluence, and pulse width, we must first numerically solve the five-band model. There is, consequently, no calculational benefit in our using the quasi three-level model. The point of calculating σ_{ex} is that we must use this to design an optimized graded density limiter.

A limiter based on excited-state absorption has a linear transmittance $T_L = \exp(-\sigma_g N_0 L)$, where N_0 is the molecular density and L the limiter length. In a three-level system the minimum possible transmittance T_{min} would occur when all molecules are in the excited state, i.e., $T_{min} = \exp(-\sigma_{ex} N_0 L)$. This is usually not attainable, as laser damage to the material typically occurs before complete excitation is reached. As we desire both a small value of T_{min} and a large value of T_L, it is appropriate to define a figure of merit (FOM) for a limiter based on excited-state absorption as FOM = T_L/T_{min} (Ref. 8), where T_{min} is the minimum transmittance for the attainable excited-state population. This definition, not accidentally, is identically equal to the DR; hence DR_{MAX} = FOM_{MAX} = $\exp[(\sigma_{ex} - \sigma_g)N_0 L]$ or,

$$DR_{MAX} = T_L^{(1-\sigma_{ex}/\sigma_g)}. \qquad (2)$$

Because the fluences required to obtain this maximum DR are not attainable, we must determine the appropriate cross sections and T_{min} from a model of excited-state absorption.

3. Effective Three-Level Cross Sections for Gradient Density and Tandem Limiters

A. Fluence Effective Cross Section σ_{eff}^F

Within the three-level approximation we can analytically solve the rate equations for the irradiance change with depth in a material as

$$\partial I/\partial z = -N_0 I\{\sigma_g \exp(-F_t/F_S)$$
$$+ \sigma_{ex}[1 - \exp(-F_t/F_S)]\}, \qquad (3)$$

where we define $F_t = \int_{-\infty}^{t} I(t')\mathrm{d}t'$ and $F_S = \hbar\omega/\sigma_g$ is the saturation fluence.[10,11] Note that in Ref. 11, $F_S = \hbar\omega/\phi\sigma_g$, where ϕ is the fraction of the excited singlet population that reaches the triplet state and σ_t is then used for the effective excited-state cross section. To make a comparison to the more accurate five-band model, we do not include ϕ in our definition of F_S. A low F_S will allow a small fluence to populate the excited state and deplete the ground state. The term in curly brackets is the effective absorption cross section for irradiance σ_{eff}^I as defined by Miles.[11] However, it is the total pulse fluence that is of primary interest. Integrating Eq. (1) over time from
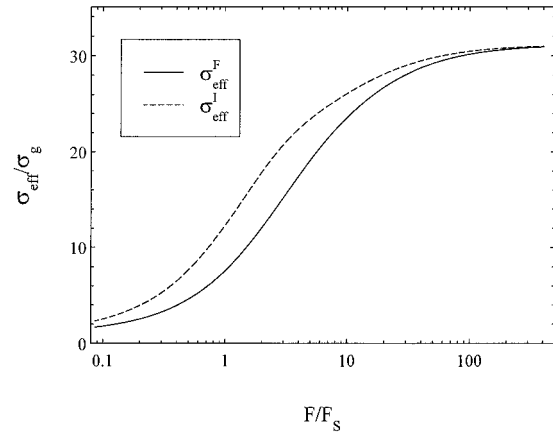

Fig. 3. Dependence of σ_{eff}^I/σ_g and σ_{eff}^F/σ_g on normalized incident fluence F/F_s for SnPc.

$-\infty$ to ∞ we find the total fluence change with z:

$$\partial F/\partial z = -\sigma_{ex}N_0 F + (\sigma_g - \sigma_{ex})[\exp(-F/F_S) - 1]N_0 F_S, \qquad (4)$$

where now an effective cross section can be defined as

$$\partial F/\partial z = -\sigma_{eff}^F N_0 F. \qquad (5)$$

In Fig. 3 we show the variation of σ_{eff}^F and σ_{eff}^I with F/F_S. The values of cross sections and level lifetimes used in the calculation are for tin phthalocyanine (SnPc), $\sigma_g = 2.1 \times 10^{-18}$ cm^2, $\sigma_s = 2.3 \times 10^{-17}$ cm^2, $\sigma_t = 6.7 \times 10^{-17}$ cm^2, $\tau_{21} = 4.44$ ns, and $\tau_{24} = 3.63$ ns (Ref. 11). In both cases, σ_{eff} saturates to its maximum possible value σ_{ex} for $F \gg F_S$, although σ_{eff}^F reaches this limiting value for considerably higher inputs. From Eq. (3), σ_{eff}^I is a monotonically increasing function of t. Therefore an average in time will always give a reduced effective cross section. As seen from the behavior of σ_{eff}^F in Fig. 3, the RSA material is not used effectively until $F > 10\,F_S$. Similarly, an average over the spatial distribution of the input pulse in r will further reduce the effective cross section for the total pulse energy. This spatial average is difficult if not impossible to perform analytically, and we only take this into account in the numerical propagation model that does show a reduction in limiting effectiveness as seen in Section 5.

For the five-level model with singlet and triplet excited-state cross sections and number densities σ_s, N_2 and σ_t, N_4, Eq. (5) is replaced by

$$\frac{\partial F}{\partial z} = -\int_{-\infty}^{\infty} [\sigma_g N_1(t') + \sigma_s N_2(t') + \sigma_t N_4(t')]I(t')\mathrm{d}t', \qquad (6)$$

which must be calculated numerically. To determine an effective three-level cross section to match the five-level model nonlinear absorption for a given pulse width and fluence, we equate Eqs. (5) and (6). Calculating σ_{eff}^F in this way reveals the pulse width dependence as well as fluence dependence of the non-
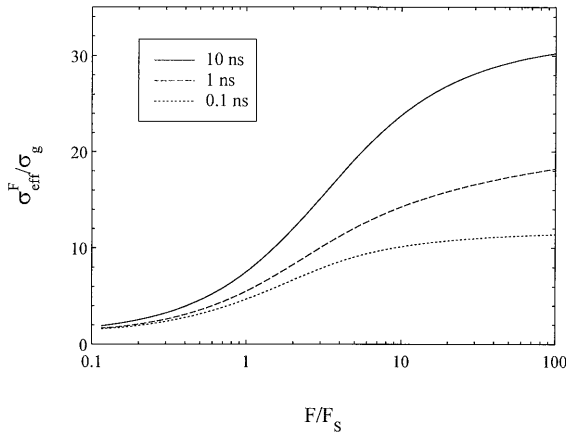
Fig. 4. Normalized effective fluence cross section $\sigma_{\text{eff}}^F/\sigma_g$ for SnPc as numerically calculated for a five-level system for several pulse widths, as a function of normalized input fluence.

linear absorber. For example, if $\sigma_t > \sigma_s$, σ_{eff}^F is lower for shorter pulses due to the time taken for decay from the singlet band to the more heavily absorbing triplet. Figure 4 shows σ_{eff}^F for several different input pulse widths, again for SnPc. The calculated F_S for this material is 0.22 J/cm². As can be seen in Fig. 4, for 10-ns pulses the RSA material is not used effectively until $F \simeq 50 F_S \simeq 10$ J/cm². A three-level model is, therefore, insufficient to describe completely the limiting properties of a five-level system. We must use the five-level model to determine a σ_{eff}^F for the purpose of design and analysis of the graded limiter for a particular pulse width and fluence. Therefore, we refer to this analysis as a quasi three-level model. An accurate calculation of the effective cross section is important because, in calculating the limiter transmittance, σ_{eff}^F appears in an exponent so that small changes make a large difference.

Figures 3 and 4 indicate that we desire as small a saturation fluence F_S as possible because this will give maximum attenuation for relatively small input fluences. Hence, from the definition of F_S, large ground-state cross sections are desired (while keeping $\sigma_e \gg \sigma_g$). For a given product $(\sigma_{ex} - \sigma_g)N_0$, it is preferable to have larger cross sections and a smaller N_0 since it takes less energy to excite fewer molecules. In addition, to reach the largest σ_{eff}, F_S should be well below F_d.

We emphasize saturation effects in the context of optimized limiters because, for the materials studied to date, damage occurs well before full saturation.[8,10] For example, solid polymer hosts currently used as hosts for RSA molecules[9] have damage thresholds of $\simeq 1$–3 J/cm² and, therefore, do not allow efficient use of the nonlinearity. This may partly explain the difference between predicted and actual performance of the limiting device of Ref. 9. It is important to ensure that every part of the limiter gives the lowest transmittance possible, i.e., be as close to saturation as possible. This means that, ideally, every part of

the limiting material should reach the damage threshold simultaneously.

In practice, reaching the saturated σ_{eff}^F is even more difficult to achieve than may be immediately apparent from this model, as the fluence may vary along two spatial directions, r and z. Along the propagation direction z, the fluence will change because of either beam focusing or absorption. This variation is removed in the graded density limiter but must be considered for constant density tandem limiter elements. There will also always be transverse fluence variations, which will reduce the effective cross section for the transmitted energy since this involves integration over the spatial beam profile. Even for uniform irradiance input beams, both linear diffraction and the presence of a nonlinear medium will distort the beam shape as it approaches focus. This cannot be rectified by a variation of the molecular concentration along z. The effects of transverse spatial variations cannot easily be considered analytically but are included in our numerical propagation model, described in Section 5.

B. Effective Cell Cross Section σ_{eff}^c

Generally σ_{eff}^F is a useful parameter to describe the limiting behavior at a single plane along the beam-propagation direction. As the fluence is constant throughout a graded density limiter, σ_{eff}^F is also useful for this specific geometry. However, to describe the composite performance of a cell of uniform molecular concentration, as in a tandem limiter, we must account for the change in the beam irradiance through the cell. All we can do here is to numerically integrate to find the transmitted fluence F_{out} for a given input F_{in}. Although this gives all the information we need, it is again useful to translate this back to an effective cross section σ_{eff}^c, which is defined by $F_{\text{out}} = F_{\text{in}} \exp(-\sigma_{\text{eff}}^c N_0 L)$, giving

$$\sigma_{\text{eff}}^c = \ln(F_{\text{in}}/F_{\text{out}})/N_0 L. \qquad (7)$$

The σ_{eff}^c is naturally smaller than σ_{eff}^F at the input plane for any given F_{in} as F must decrease through the cell. For this reason, as discussed in Section 4, tandem limiters are more efficient if they are constructed of many cells, each of high linear transmittance, so that the decrease in F through each cell is small. The limit of this, as the number of cells becomes large, is the graded density limiter, as discussed in the next section.

4. Relative Performance of Graded Density and Multicell Tandem Optical Limiters

Limiters using discrete nonlinear elements (of spatially uniform concentration) in tandem have been previously proposed[8,16] and demonstrated.[8,9,16] The motivation for designing such tandem or multicell optical limiters was primarily to provide a large extension of the DR while keeping the limiting threshold as low as possible and the linear transmittance as high as possible. However, as shown below, and as discussed by Miles[11] from a different viewpoint, the

multicell limiter can function as a good approximation to the optimized graded limiter. The principle of the tandem limiter is that each discrete element is positioned so that it will protect the next element from damage. As for the graded density limiter, the nonlinear elements are positioned on the -z side of the focal plane and for optimized behavior are positioned so that they will all reach their damage threshold for the same input energy. In this section we describe the performance and design considerations for tandem and graded density limiters. This analysis treats a Gaussian input beam assumed to remain Gaussian throughout the propagation in z. The assumption of a radially uniform (top-hat) beam yields similar results.[11] However, as discussed in Section 5, numerical solutions properly including diffraction show significantly poorer limiting performance. In either case, we can expect aberrations to dominate the beam shape near the focus in an imaging system with f/No. smaller than $\simeq 5$. Inclusion of aberrations would require knowledge of the details of a specific imaging system and so are omitted from this analysis which is therefore limited to f/#'s > 5.

A. Graded Density Limiters

Although tandem limiters historically preceded the idea of graded limiters, we discuss the graded variety first, as they offer the greatest simplicity, and much of what we conclude about these will also apply to tandem limiters. To maximize the nonlinear absorption for the highest possible input, all portions of the nonlinear material should be at or very near to the damage threshold. This implies that the fluence is a constant with z as long as the damage threshold is independent of z. We assume this to be true so that

$$\left.\frac{\partial F}{\partial z}\right|_{F=F_d} = 0. \qquad (8)$$

As the output fluence from a ESA limiter is a monotonically increasing function of the input fluence, then with this design the maximum transmitted fluence must also be F_d. The criterion of Eq. (8) can be achieved in absorbing media when a beam is focused so that the increase in fluence with propagation exactly balances the decrease in fluence that is due to absorption, or

$$\frac{\partial F}{\partial z} = \left.\frac{\partial F}{\partial z}\right|_D + \left.\frac{\partial F}{\partial z}\right|_A = 0, \qquad (9)$$

where subscripts D and A refer to diffraction (in this case focusing) and absorption, respectively. Although graded limiters have been analysed elsewhere,[10,11] we include the following abbreviated derivation for completeness.

Fortunately, we do not need to solve Eq. (4) to optimize the limiting if we consider the following simple arguments. Using Eq. (4) in Eq. (9) and assuming the beam always follows Gaussian beam propagation {i.e., $F_D(z) = F_D(0)[1 + (z/Z_0)^2]$}, we find by differentiation that the following molecular distribution is needed:

$$N_0(x) = -\frac{x}{1+x^2}\frac{2}{\sigma_g Z_0}\frac{1}{\Sigma} \text{ for } x < 0, \qquad (10)$$

where $x = z/Z_0$ and $\Sigma = (\sigma_{\text{eff}}^F/\sigma_g)$. This distribution reduces to that given by Miles[11] $[N_0(z) \simeq 2/(z\sigma_{\text{ex}})]$ for large F/F_s and $z_1, z_2 \gg Z_0$, where z_1 and z_2 are the positions of the entrance and exit surfaces of the limiter. With this density function we can determine the remaining design parameters of the limiter. First, we must specify the optical system, namely the wavelength λ and beam waist w_0. Our material will define Σ and F_d, so we are left to specify a maximum transmitted energy E_{out} and the linear transmittance T_L. This is sufficient information to calculate the limiter geometry, which also determines the input damage energy E_m. Typically, E_{out} will be chosen to be of the order of 1 μJ.[1] Defining the normalized position of the surfaces of the limiter by $x_i = z_i/Z_0$, we can give the linear transmittance of the material by

$$T_L = \exp\left[-\int_{z_1}^{z_2} N_0(z)\sigma_g dz\right] = \left(\frac{1+x_2^2}{1+x_1^2}\right)^{1/\Sigma}. \qquad (11)$$

As the beam is assumed to remain Gaussian but the on-axis fluence is constant, E_m and E_{out} are related by

$$E_m = \left(\frac{1+x_1^2}{1+x_2^2}\right)E_{\text{out}} = E_{\text{out}}T_L^{-\Sigma}. \qquad (12)$$

As expected, the minimum transmittance is given by $T_{\text{min}} = E_{\text{out}}/E_m = T_L^{\Sigma}$. We therefore obtain the DR as

$$\text{DR} = T_L^{(1-\Sigma)}, \qquad (13)$$

which, in the limit of $F \to \infty$, converges to $\exp[(\sigma_{\text{ex}} - \sigma_g)N_0 L]$, in agreement with Eq. (2).

The positions x_1 and x_2, both negative, are determined by

$$x_1^2 = F_p/F_d - 1, \quad x_2^2 = T_L^{\Sigma}F_p/F_d - 1, \qquad (14)$$

where $F_p = 2E_m/\pi w_0^2$ is the fluence at focus in the absence of nonlinear material.

An examination of the above results reveals that the effect of specifying the fluence as a function of z is to impose hard constraints on the design of the limiter. This also places well-defined limits on what we can expect of the performance of an optimized device, be it of the graded or tandem variety.

First, this limiter design intrinsically places a limit on how small the transmitted energy can be when operating at maximum fluence F_d. Equation (14) yields general values for the positions of the front and rear surfaces of the limiter when linear transmittance T_L, cross-sectional ratio $\Sigma = \sigma_{\text{eff}}^F/\sigma_g$, spot size w_0, and either maximum input or transmitted energies E_m or E_{out} are specified. As the on-axis fluence

is F_d for all z, then

$$E_{\text{out}} = \frac{\pi F_d}{2} w_0^2 (1 + x_2^2). \tag{15}$$

For most applications, this is a more general relationship than needed. This is because E_{out} is minimized for $x_2 = 0$ and, as we shall see, we will nearly always want to set $x_2 = 0$ to obtain this minimum as long as material nonlinearities remain low. Setting $x_2 = 0$ yields

$$E_{\text{out}} = \frac{2}{\pi} F_d \lambda^2 (f/\#)^2, \tag{16}$$

where the (f/No.) is defined here as the ratio of the focal length of the input lens to the beam diameter ($1/e^2$ in irradiance) at the lens. Note that E_{out} is independent of the material's nonlinear properties, depending only on the maximum fluence F_d and the focusing geometry. For eye protection, a reasonable upper value for E_{out} is $\simeq 1$ μJ.[11] From Eq. (7) we find that this can be achieved for an $f/10$ limiter only if $F_d \leq 5$ J/cm^2 and for an $f/5$ limiter if $F_d \leq 20$ J/cm^2. From our results in Section 3, we can see that, to reach the necessary effective cross sections in currently available materials, the fluences must be considerably greater than 5 J/cm^2. In the event that ESA materials are developed with saturation fluences considerably lower than those currently available, requirements on the value of F_d can be reduced, allowing the rear limiter surface to be moved away from focus without increasing E_{out}. This would allow the use of materials with lower damage thresholds.

Another constraint is that the design length can become prohibitively long if Σ is large. Equation (14) gives the locations x_1 and x_2 of the front and rear surfaces of the limiter, from which the device length $L = (x_1 - x_2) Z_0$ can be found. Again, setting $x_2 = 0$, we find a relatively simple expression for the sample length:

$$L = Z_0 (T_L^{-\Sigma} - 1). \tag{17}$$

The strong dependence of L on both Σ and T_L is seen by examination of Fig. 5, where we plot the normalized limiter length L/Z_0 as a function of T_L for several values of Σ. From Eq. (13), we can see that reducing T_L by a small amount may drastically increase the DR. With such an increase in the DR, a small reduction in T_L may in itself be tolerable. However, the consequential increase in limiter length may not be. For example, with $\Sigma = 25$, a decrease in T_L from 0.8 to 0.6 results in a decrease in T_{min} by a factor of 10^3, while L changes from 260 Z_0 to 3×10^5 Z_0. This length dependence is because $N(z)$ is predetermined so that the only way to change T_L is to change the limiter length, and far from focus, $N(z)$ becomes very small. In Fig. 6 we use Eq. (17) to plot T_{min} versus T_L for several values of Σ. Correspondingly, we can see from Fig. 5 that a large Σ for a given T_L also requires a large L. This is because the larger
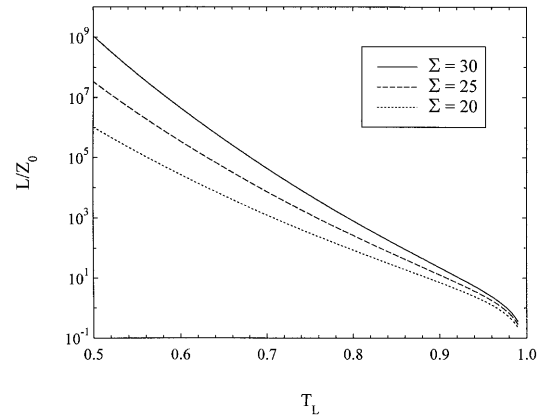
Fig. 5. Graded limiter length L in units of Z_0 versus linear transmittance T_L for several values of Σ.

Σ is, the more dilute the molecules must be to satisfy Eq. (8) for a given f/No.

Our numerical beam-propagation calculations, described in Section 5, have shown that, although the constant beam shape approximation is helpful in designing limiting devices, the energy transmittance can be more than an order-of-magnitude greater than analytically predicted. Moreover, the effect of nonlinear refraction, both from the refractive contribution of excited states and from heating of the host material, may further increase the transmitted energy. This has yet to be modeled.

The subject of gradient density limiters is currently entirely theoretical; to date we have no means of making them. Although it is highly speculative as to which technology may eventually be used to maintain such a molecular density gradient, we can be reasonably certain that the molecules would be held in a solid host rather than a liquid solution. This may lead to severe constraints due to optically induced damage, which, for example, in a polymer host is of the order of 3 J/cm^2.[9,11] This severely restricts the values of Σ that could be achieved and hence constrain the DR of the limiter. Liquid solutions
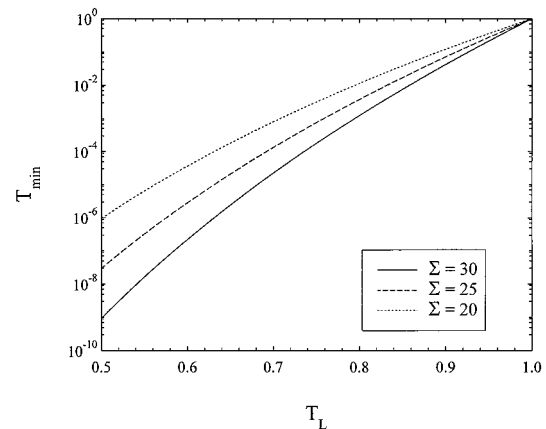

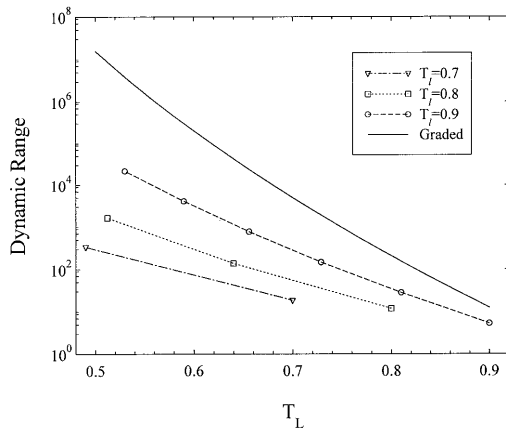Fig. 6. Transmittance at maximum input versus linear transmittance T_L for several values of Σ.

Fig. 7. Dynamic range, or figure of merit, versus T_L for a graded limiter and several tandem limiters with cell linear transmittance T_l, based on the material parameters of SnPc.

Fig. 8. Effective cell cross section σ_{eff}^c versus fluence for several values of cell linear transmittance T_l.

held in quartz containers, on the other hand, have been shown to have damage thresholds of 50 J/cm^2 or greater,[12] so that the maximum fluence allowed by Eq. (7) can be easily reached. Of course, a graded distribution cannot be maintained in a liquid, which points us, once again, to tandem limiters.

B. Tandem Limiters

As implied by Fig. 1, the general behavior of a multielement tandem limiter is similar to that of a graded density limiter. For a multielement limiter comprised of n discrete elements, assuming a constant beam shape, the DR is given by[8]

$$\text{DR} = \prod_{j=1,n} \left(\frac{T_{lj}}{T_{mj}} \right), \tag{18}$$

where T_{lj} and T_{mj} are the linear and minimum energy transmittances for the jth element, and hence (T_l/T_m) is the DR for each element. Should all elements be identical, Eq. (18) reduces to

$$\text{DR} = \left(\frac{T_l}{T_m} \right)^n. \tag{19}$$

The relationship between tandem and graded concentration limiters is shown in Fig. 7. The DR is plotted versus T_L for tandem limiters comprised of cells, all with $T_L = 0.9$, $T_L = 0.8$, or $T_L = 0.7$. For each type of cell, the DR of various numbers of elements is plotted with Eq. (18). Also plotted is the DR of the optimized, graded distribution limiter, as calculated by Eq. (13). Clearly, the trend indicates that a tandem limiter with a large number of elements, each of high linear transmittance, becomes equivalent to the graded concentration limiter as $n \to \infty$. This is not surprising, as the tandem limiter design requires that the reduction in fluence by absorption in each element must equal the increase in fluence by linear propagation between the elements. This is exactly the same requirement as Eq. (2) for the graded distribution limiter, except on-axis fluence oscillates be-
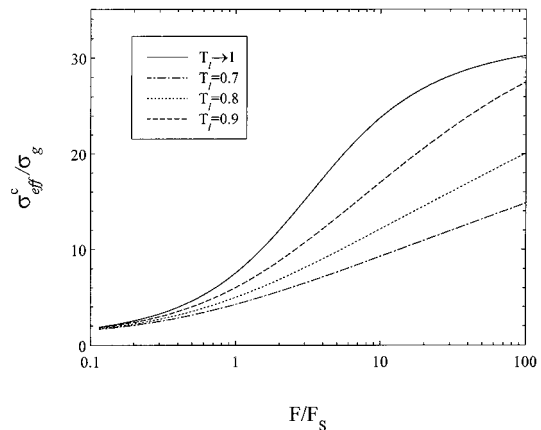
tween F_d and $T_{\min} F_d$ in this discrete system, as shown in Fig. 1. This is why we must use σ_{eff}^c, defined in Eq. (7), as the effective cross section in the tandem limiter.

Because the fluence decreases through each cell, the nonlinearity near the rear surface of each cell is much harder to saturate than near the front surface. This makes it even more difficult to reach saturation in the multicell limiter than in the graded limiter. Defining $S = \sigma_{\text{eff}}^c/\sigma_g$, $T_m = (T_l)^S$, so that the DR for an individual cell is $(T_l)^{1-S}$, in Fig. 8 we plot the calculated value of S from the five-level model as a function of input fluence for several values of linear cell transmittance T_l. This is done in the approximation that the effects of diffraction are negligible within the cell. Also plotted in Fig. 8 is the parameter Σ for the graded concentration limiter, illustrating that Σ is the limit of S as $T_l \to$ unity and the number of cells becomes large. To fully utilize the entire thickness of an individual cell, as shown in Fig. 8, two things are important. The linear transmittance of each individual cell must be kept close to unity, and the fluence should be as high as possible. This requires high F_d/F_S, again indicating that it is important to design a multicell limiter so as to give as high a damage threshold as possible. Our studies reveal that the best host for RSA molecules is a liquid solvent in a high-grade fused-silica cell. These cells can have a damage threshold as high as $\simeq 400 \text{ J/cm}^2$.[4]

The minimum energy transmittance for the entire limiter must be given by $T_{\min} = T_m^n$, where n is the number of cells. Similarly, the total linear transmittance is $T_L = T_l^n$. Combining these statements, we conclude that, for the multicell limiter, the DR $= T_L^{(1-S)}$. Note the similarity between this equation and Eq. (13) for the DR of the graded concentration limiter.

We can now design the multicell limiter. It is straightforward to show that the normalized distance from focus x_1 of the first cell is given by

$$x_1 = \sqrt{F_p/F_d - 1}. \tag{20}$$

For the next and remaining cells,

$$x_j = \sqrt{(1 + x_{j-1}{}^2)T_{m(j-1)} - 1}, \qquad (21)$$

where w_j is the beam radius at the jth cell, with $j = 1, 2, \ldots, n$.

Although decreasing fluence through the cell results in reduced efficiency, an obvious benefit is that E_{out} is simultaneously reduced. By analogy with Eq. (16), we find that for the tandem limiter

$$E_{\text{out}} = \frac{2}{\pi} F_d \lambda^2 (f/\#)^2 T_{\min}(1 + x_n{}^2), \qquad (22)$$

where x_n is the position of the final cell. Again, placing the final cell at focus, $x_n = 0$ and E_{out} is minimized.

It was suggested in Ref. 11 that one may wish to make the final element thick, so that the fluence may rise back up to F_d at the exit surface as the beam focuses, as shown by McCahon and Tutt.[17] This results in a minimum output energy for the particular geometry, while remaining below the damage threshold. However, it does not provide a globally minimized transmitted energy for a fixed linear transmittance, which occurs with the last sample positioned at focus. With the final (nth) cell at focus, we are specifying $w_n{}^2 = w_0{}^2$, and the position of the other cells is found in a manner similar to Eq. (21), using $w_{j-1}{}^2 = w_j{}^2/T_{m(j-1)}$.

As an example, we describe the design of a multicell limiter for a $f/5$ system at a wavelength of 532 nm, where we require $E_{\text{out}} \leq 1$ μJ and an overall linear transmittance of 70%. Assuming a damage fluence of 50 J/cm², as is possible for liquid-filled fused-silica cuvettes, we have $F/F_S = 267$ at the input surface of each cell. For this fluence in SnPc we calculate from the five-level model $\sigma_{\text{eff}}{}^F = 6.5 \times 10^{-17}$ cm², indicating significant, though not total, triplet occupation [$\sigma_t = 6.7 \times 10^{-17}$ cm² (Ref. 11)]. We find that we can meet the design requirements with a four-cell device, three with $T_l = 0.92$ and the final one with $T_l = 0.90$. For these values, we can find S either from Fig. 8 or by direct calculation. Using $T_{\min} = T_L{}^S$, we find $T_{\min} = 1.9 \times 10^{-5}$.

Assuming no aberration, the calculated beam waist is small enough that E_{out} is well below the requirement and hence $E_{\max}$ is unnecessarily low. For this reason, we calculate the position x_4 of the final element by specifying $E_{\text{out}} = 1$ μJ in Eq. (22). (In reality, aberrations would require this position to be nearer to or at focus.) This value of x_4 and corresponding values for x_1, x_2, and x_3 calculated from Eq. (21) gives a maximum input energy of $E_{\max} = 52$ mJ and a DR of 36,500.

The performance of the four-cell device is close to optimum if the fluence is sufficiently high. For example, with $F_d = 50$ J/cm² and the same T_L, we calculate $\Sigma = 31$ for $F/F_S = 267$, giving a DR of 45,000, only approximately 20% better than the four-cell device. As the graded limiter, the dependence of performance on T_L is strong. For example, if we

allow T_L to drop slightly from 70 to 60%, $T_{\min}$ drops by a factor of 110, allowing an $E_{\max}$ of almost 5.8 J for a 1-μJ output energy and a corresponding DR of 3.5×10^6. A consequence is that the limiter length goes from 152 Z_0 (3.86 mm) to 1600 Z_0 (40.7 mm). Unfortunately, as discussed in the next section, these analytical calculations are overly optimistic.

5. Numerical Propagation Model

The assumption that a beam should retain its shape while propagating through a nonlinear material over many diffraction lengths was initially made with little justification. Indeed, we can be certain that the beam will not remain Gaussian (or any other assumed constant shape), but we cannot tell analytically how far this removes our design from the optimum case. As this is critical to the design of the optimized limiter, it is necessary to verify its operation, either experimentally or numerically. Although experiments ultimately provide the best evidence, a numerical code to model these systems allows great flexibility, as we can adjust material and geometric parameters at will so as to gain insight on the operation of the limiter. Also, for graded density limiters, a means of creating the graded molecular concentration that precisely follows some mathematical function has not yet been established. For these reasons, we wrote a numerical code to determine the nonlinear propagation by solving the wave equation.

To meet our goals, we had to construct a code robust enough to propagate a beam through a highly nonlinear medium over distances of several hundred Z_0. The method chosen to satisfy these criteria was patterned after that of Feit and Fleck.[18] The method is based on the paraxial approximation and slowly varying envelope approximation, both valid in our studies with $f/10$ or $f/5$ optics and pulses of durations in the tens of picoseconds to nanosecond ranges. This method utilizes fast Fourier transforms to solve the wave equation in the evolution operator form. We see how this can be applied by rewriting the scalar wave equation in the form

$$\frac{\partial}{\partial z}\Psi(r, z, t) = \frac{1}{2ik}(\nabla_T{}^2 + k_0{}^2\chi_{NL})\Psi(r, z, t), \quad (23)$$

which has an evolution operator solution

$$\Psi(r, z + \Delta z, t) = \exp\left[\int_z^{z+\Delta z} S(z')dz'\right]\Psi(r, z, t), \quad (24)$$

where operator S is given by

$$S(z') = \frac{1}{2ik}[\nabla_T{}^2 + k_0{}^2\chi_{NL}(z')]. \qquad (25)$$

The operator S may be applied by a Taylor-series expansion of the exponential in Eq. (24), as described in detail in Refs. 18 and 19. Then the derivatives can be calculated by expansion of the field in a Fou-
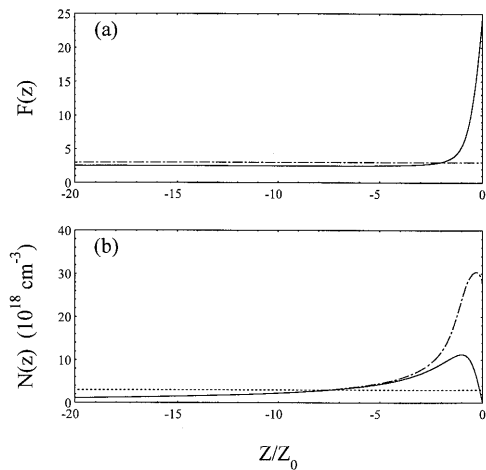
Fig. 9. (a) Calculated on-axis fluence as a function of z for the analytically determined molecular distribution of Eq. 10 (solid curve) and the numerically optimized graded density limiter (dashed curve). The fluence at the input to both distributions (at $z/Z_0 = -135$) is 3 J/cm^2. (b) Analytically (solid curve) and numerically (dashed curve) calculated molecular distributions for the graded density limiter.
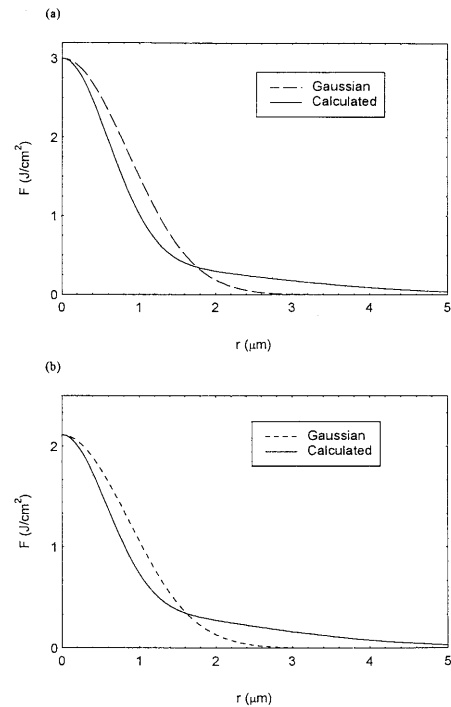

Fig. 10. (a) Radial distribution of fluence at the output of the graded density limiter, as calculated by the numerical propagation code as compared with a Gaussian. (b) Radial distribution of fluence at the output of the four-element tandem limiter, as calculated by the numerical propagation code as compared with a Gaussian.

rier series.[18] The use of cylindrical symmetry, valid for most limiting applications, means that the code can run much faster than a full three-dimensional code. The accuracy can also be much higher than split step and fast Hankel transform solutions[20] that are accurate to $(\Delta z)^3$, where Δz is the incremental element in the propagation direction. By arbitrary truncation of the expansion of the evolution operator, the accuracy can be to arbitrary order in Δz. Usually we use $(\Delta z)^4$ to $(\Delta z)^6$.[21] This accuracy allows propagation through large distances, over which the change in beam size can be enormous. For large changes in the transverse spatial dimension, a varying grid size and interpolation is used to optimize the computer run time. The resulting program is capable of computing Gaussian propagation over $10^3\, Z_0$ with less than a 10^{-5} error in the on-axis irradiance.

We have applied this program to the calculation of beam propagation in both graded density and tandem devices, where we have used SiPc as an example.[11] Figure 9(a) shows the results of a test of the optimized graded density limiter, where we plot the calculated on-axis fluence versus z for a $f/5$ focusing system. The parameters used are the same as used for Fig. 4.[11] The design parameters for this material and f/No. are calculated from Eqs. (14)–(17) to be $T_L = 0.7$, $E_{out} = 7$ μJ, $x_1 = -135$ and $x_2 = -5$, $E_{max} = 5$ mJ, $F_d = 1.5$ J/cm^2, $w_0 = 3.4$ μm, and $\lambda = 532$ nm.

The input beam was assumed to have a Gaussian spatial profile at a wavelength of 532 nm and Gaussian temporal pulse width of 10 ns (FWHM). The damage threshold is chosen as 3 J/cm^2 to match the possible damage to solid-state hosts.[9,11] With this focusing geometry, $Z_0 = 170$ μm, which for a 2-cm-thick sample requires calculation for over 100 Z_0. The calculated on-axis fluence is shown in Fig. 9(a) for the range $z = -20\, Z_0$ to $z = 0$ ($x = -20$ to 0). The

solid curve in Fig. 9(a) shows clearly that propagation effects cause the on-axis fluence to deviate from the analytically assumed value. However, it is possible to find an optimized distribution by use of the numerical code itself. To keep the fluence below the damage threshold, the program iteratively adjusts the molecular density at each z position. Figure 9(b) shows that this optimized molecular density follows the analytical density [Eq. (10)] well until near the focal region where it turns up sharply by a factor of $\simeq 3$. Unfortunately, this optimized density distribution is material and geometry dependent so that for each system, a separate run of the beam-propagation code must be performed to determine the optimized distribution. The dashed curve in Fig. 9(a) is the on-axis fluence for the numerically optimized limiter.

Observing the radial distribution of the fluence at the output of the analytically determined graded density limiter, shown in Fig. 10(a), we find there is a moderate distortion of the beam shape due to the nonlinear absorption. This distortion results in a three-fold increase in E_{out}, compounded with the increase in fluence above the design value, in this case a factor of 2. Hence the transmitted energy for the analytically determined molecular distribution is a factor of 6 greater than the designed value. In addition we see an apparent beam narrowing, but considerable energy is scattered to the wings. For a single element we would expect beam broadening since the peak is more strongly absorbed. There-
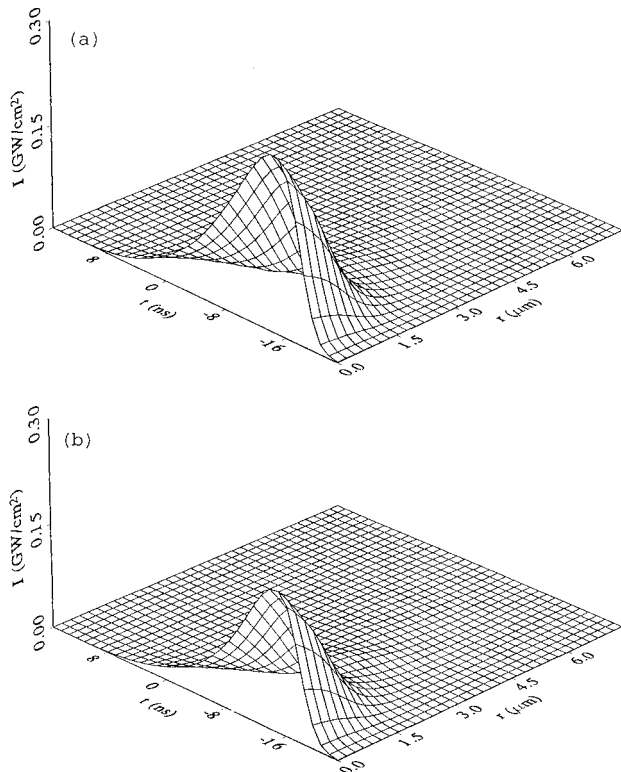
Fig. 11.   (a) Numerically calculated irradiance at the output of the optimized graded density limiter, as a function of radial position and time for a spatially and temporally Gaussian input.   Note that the output is greatly advanced in time as expected for a fluence limiter.   (b) Output irradiance distribution for the four-element limiter, as calculated by the numerical propagation code.

Fig. 12.   (a) Numerically calculated on-axis fluence for the four-element limiter as a function of z/Z_0, as calculated with the numerical beam-propagation code.   The material and geometric parameters are the same as used for Fig. 1, which was calculated assuming a constant beam shape.   (b) Detail of Fig. 12(a) near the focal plane.   Note that in the final nonlinear element, the fluence reaches a minimum and starts to increase with z, as predicted in Refs. 11 and 17.

fore, the propagation appears to be an important factor (i.e., the beam broadening reduces diffraction).

In Fig. 11(a) we show the irradiance distribution at the output of the graded density limiter as a function of both time and space.   For larger values of $\sigma_{eff}^{F}/\sigma_g$ we observe that the distortion becomes larger, primarily due to the necessary increase in limiter length.   Numerically calculated energies to 20 times the analytically predicted values are observed in our studies.   This further emphasizes the usefulness of numerical propagation in the design process.   Inclusion of nonlinear refraction, from both excited state and thermal sources, can be expected to cause considerable further distortion.

The numerical code is also useful in calculating the behavior of the tandem limiter.   A simple diffraction integral is adequate for calculation of propagation between the elements far from focus, where the thin sample approximation may be valid for propagation between the elements.   However, near focus, the thin-sample approximation is seen to break down, and propagation between elements may require a large enough number of points that use of the fast Fourier transform method is desireable.   In Fig. 12, we show the on-axis fluence for the four-element tandem limiter, described in Section 4 and shown in Fig. 1, under the Gaussian shape approximation.
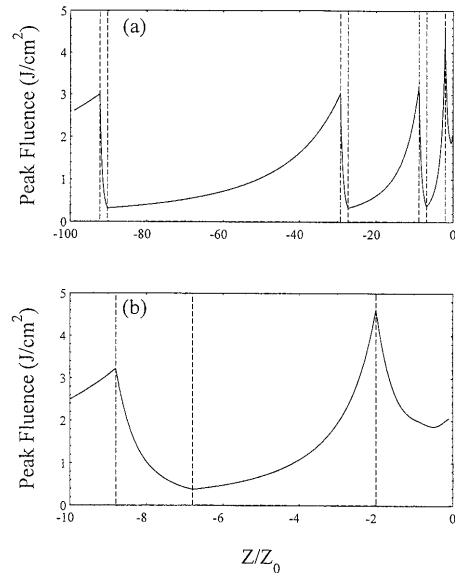
Clearly, the analytic method works well for the first three elements, with deviations from the analytically predicted propagation only becoming apparent near the final element.   Even there, the deviations from predicted behavior are small.   Note that the fluence is seen to reach a minimum within the last element after which it starts to increase with z, as predicted in Refs. 11 and 17.   The calculated output fluence distribution for this limiter is shown in Fig. 10(b) and the corresponding irradiance distribution is given in Fig. 11(b).

Finally, in Fig. 13 we show a comparison of the numerically calculated FOM with the analytic values, for both graded density and tandem limiters.   Again the material parameters are those for SnPc.   The numerical determination of the FOM is based on calculated energy transmittance.   As expected, the actual behavior deviates more strongly from the analytic approximation as the transmittance is decreased (and hence the limiting behavior becomes stronger).   As T_L approaches 50%, the actual performance may be as much as two orders of magnitude poorer than the analytic prediction.   The effects of nonlinear refraction can be expected to further degrade the limiting performance, but the degree to which this is true is as yet undetermined.

6.   Conclusion

For optimization of both tandem and graded density limiters the goal as discussed in this paper is to attain the maximum dynamic range or FOM.   For tandem limiters, the elements are placed upstream in just
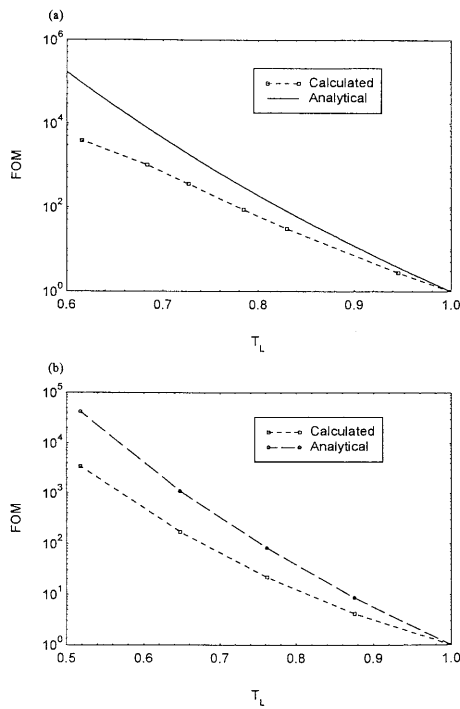
Fig. 13. Comparison between analytically and numerically determined figures of merit for (a) graded density and (b) four-element tandem limiters, as a function of T_L.

such a way as to protect the next element downstream (and closer to focus) from damage. Thus, at the highest input, each element operates at the damage threshold (actually just below the damage threshold). Here the front surface of each element operates at threshold, but within any element the fluence drops due to absorption, and is, therefore, not optimally utilized. For the graded density limiter each portion Δz (differential element along the propagation direction) of nonlinear material protects the downstream portion from damage; thus, all the nonlinear material operates at the damage threshold. The original motivation for the tandem limiter was to keep a low limiting threshold but increase its dynamic range. The motivation for the graded density limiter (see Ref. 11) was to ignore the threshold and low-input operation, look only at the high-energy input, and keep the output for this input below a fixed value determined by damage to optical components. In the end, the two viewpoints give identical results for tandem limiting. In addition, in the limit where the number of elements in a tandem limiter becomes large, the difference between a tandem limiter and a graded density limiter vanishes.

The optimization procedure, here applied to ESA materials, can be applied to other nonlinear processes. This is particularly simple for pure 2-photon absorption (2PA) materials governed by $dI/dz = -\beta(z)I^2$, where $\beta(z)$ is the 2PA coefficient, allowed to vary with molecular concentration along z. Here the assumption is that the irradiance rather than fluence is held constant with z. The resultant density dis-

tribution is then given by $\beta(z) = -2x/[(1 + x^2)I_dZ_0]$, where I_d is the damage threshold for the irradiance. The z dependence is the same as for ESA materials, showing the close connection between the two linear absorption processes for excited-state absorption and the single-step 2PA process. A possible advantage for a 2PA-based limiter, if the large β's needed could be found, would be that it does not require linear absorption to initiate the nonlinear absorption. The numerical propagation code is also capable of optimizing limiting devices with use of other nonlinear mechanisms or a combination of nonlinear mechanisms. Of particular interest is the use of materials that exhibit 2PA and excited-state absorption from the 2PA populated state. Such nonlinearities have been observed in organics as well as in semiconductors.[22]

There are several restrictions on the use of the analysis presented here that must be discussed, both for the analytical and numerical modeling. For low f/No., aberrations in optical systems may alter the propagation from the diffraction-limited performance assumed here. Inclusion of aberrations requires knowledge of the specific imaging system and therefore has not been addressed here. We conclude that this analysis, both analytical and numerical, will only be valid for diffraction-limited performance that should be valid for f/No.'s larger than approximately $f/5$. In addition, particularly for liquid-based limiters, thermal lensing may be a significant contributor to propagation near focus for pulses of the order of or longer than the acoustic transit time across the beam waist. Our initial experiments have already shown that such thermal effects are significant even for 10-ns pulses in tight focusing geometries at high inputs. This needs to be incorporated into numerical models in the future. To do this correctly will be extremely computer-time intensive as it requires simultaneous solutions of the acoustic-wave equation with the electromagnetic wave equation. We hope that approximations can be found that will allow further refinements in the design of practical limiting devices.

References

1. G. L. Wood, W. W. Clark, M. J. Miller, G. J. Salamo, and E. J. Sharp, "Evaluation of passive optical switches and limiters," in *Materials for Optical Switches, Isolators, and Limiters*, M. J. Soileau, ed., Proc. SPIE **1105,** 154–180 (1989).
2. L. W. Tutt and T. F. Boggess, "A review of optical limiting mechanisms and devices using organics, fullerenes, semiconductors and other materials," Prog. Quantum Electron. **17,** 299–338 (1993).
3. K. Mansour, E. W. Van Stryland, and M. J. Soileau, "Nonlinear optical properties of carbon black suspensions," J. Opt. Soc. Am. B **9,** 1100–1109 (1992).

4. A. A. Said, T. Xia, A. Dogariu, D. J. Hagan, M. J. Soileau, E. W. Van Stryland, and M. Mohebi, "Measurement of the optical damage threshold in fused quartz," Appl. Opt. **34,** 3374–3376 (1995).

5. D. J. Hagan, E. W. Van Stryland, M. J. Soileau, and Y. Y. Wu, "Self-protecting semiconductor optical limiters," Opt. Lett. B **13,** 315–317 (1988).

6. E. W. Van Stryland, Y. Y. Wu, D. J. Hagan, M. J. Soileau, and K. Mansour, "Optical limiting with semiconductors," J. Opt. Soc. Am. **5,** 1980–1989 (1988).

7. T. H. Wei, D. J. Hagan, M. J. Sence, E. W. Van Stryland, J. W. Perry, and D. R. Coulter, "Direct measurements of nonlinear absorption and refraction in solutions of phthalocyanines," Appl. Phys. B **54,** 46–51 (1992).

8. D. J. Hagan, T. Xia, A. A. Said, T. H. Wei, and E. W. Van Stryland, "High dynamic range passive optical limiters," Int. J. Nonlinear Opt. Phys. **2,** 483–501 (1993).

9. K. Mansour, C. T. Chen, S. R. Marder, J. W. Perry, and P. Miles, "Demonstration of strongly saturated multiple plate optical limiter based on excited state absorbers," in *Conference on Lasers and Electro-Optics*, Vol. 8 of 1994 OSA Technical Digest Series (Optical Society of America, Washington, D.C., 1994), p. 418.

10. D. J. Hagan, T. Xia, A. A. Said, A. Dogariu, and E. W. Van Stryland, "Optimization of reverse saturable absorber limiters: material requirements and design considerations," in *Materials for Optical Limiting*, R. Crane, K. Lewis, E. Van Stryland, and M. Khoshnevisan, eds., MRS Symp. Proc. **374,** (Materials Research Society, Boston, 1995), pp. 161–172.

11. P. A. Miles, "Bottleneck optical limiters: the optimal use of excited-state absorbers," Appl. Opt. **33,** 6965–6979 (1994).

12. D. R. Coulter, V. M. Miskowski, J. W. Perry, T. H. Wei, E. W. Van Stryland, and D. J. Hagan, "Optical limiting in solutions of metallo-phthalocyanines," in *Materials for Optical Switches, Isolators, and Limiters*, M. J. Soileau, ed., Proc. SPIE **1105,** 42–51 (1989).

13. J. S. Shirk, R. G. S. Pong, F. J. Bartoli, and A. W. Snow, "Optical limiter using a lead phthalocyanine," Appl. Phys. Lett. **63,** 1880–1882 (1993).

14. C. R. Guliano and L. D. Hess, "Nonlinear absorption of light: optical saturation of electronic transitions in organic molecules with high intensity laser radiation," IEEE J. Quantum Electron. **QE-3,** 358–367 (1967).

15. M. Sheik-Bahae, A. A. Said, T. H. Wei, D. J. Hagan, and E. W. Van Stryland, "Sensitive measurement of optical nonlinearities using a single beam," IEEE J. Quantum Electron. **QE-26,** 760–769 (1990).

16. A. A. Said, T. H. Wei, J. R. DeSalvo, M. Sheik-Bahae, D. J. Hagan, and E. W. Van Stryland, "Self-protecting optical limiters using cascaded geometries," in *Nonlinear and Electro-Optic Materials for Optical Switching*, M. Soileau, ed., Proc. SPIE **1692,** 37–44 (1992).

17. S. W. McCahon and L. W. Tutt, "Optical Limiter Including Optical Convergence and Absorbing Body with Inhomogeneous Distribution of Reverse Saturable Material," U.S. Patent 5,080,469 (14 January 1992).

18. M. D. Feit and J. A. Fleck, Jr., "Simple spectral method for solving propagation problems in cylindrical geometry," Opt. Lett. **14,** 662–664 (1989).

19. J. A. Fleck, J. R. Morris, and M. D. Feit, "Time-dependent propagation of high energy laser beams through the atmosphere," Appl. Phys. **10,** 129–160 (1976).

20. S. C. Sheng, "Studies of Laser Resonators and Beam Propagation Using Fast Transform Methods," Ginzton Laboratory report no. 3106 (Stanford University, Stanford, Calif., 1980).

21. T. Xia, "Modeling and experimental studies of nonlinear optical self-action," Ph.D. dissertation (University of Central Florida, Orlando, Florida, 1994).

22. A. A. Said, C. Wamsley, D. J. Hagan, E. W. Van Stryland, B. A. Reinherdt, P. Roderer, and A. G. Dillard, "Third and fifth order optical nonlinearities in organic materials," Chem. Phys. Lett. **228,** 646–650 (1994).